Nano Research 2018, 11(5): 2836–2846
https://doi.org/10.1007/s12274-017-1914-7
Research Article
ISSN 1998-0124
CN 11-5974/O4

Embedding hollow Co_3O_4 nanoboxes into a three-dimensional macroporous graphene framework for high-performance energy storage devices

Mengping Li[1], Maher F. El-Kady[1,2], Jee Y. Hwang[1], Matthew D. Kowal[1], Kristofer Marsh[1], Haosen Wang[1], Zhijuan Zhao[1], and Richard B. Kaner[1,3] (✉)

[1] *Department of Chemistry and Biochemistry and California NanoSystems Institute, University of California, Los Angeles, Los Angeles, CA 90095, USA*
[2] *Department of Chemistry, Faculty of Science, Cairo University, Giza 12613, Egypt*
[3] *Department of Materials Science and Engineering, University of California, Los Angeles, Los Angeles, CA 90095, USA*

Received: 24 August 2017
Revised: 8 October 2017
Accepted: 7 November 2017

KEYWORDS
supercapacitor,
graphene,
cobalt oxide,
laser,
composite,
hybrid capacitor

ABSTRACT

Carbon materials are widely used for supercapacitor applications thanks to their high surface area, good rate capability, and excellent cycling stability. However, the development of high energy density carbon supercapacitors still remains a challenge. In this work, hollow Co_3O_4 nanoboxes have been embedded into three-dimensional macroporous laser-scribed graphene (LSG) to produce composite electrodes with improved electrochemical performance. Here, Co_3O_4 provides high capacity through fast and reversible redox reactions, while LSG serves as a conductive network to maintain high power. The open nanobox morphology is a unique solution for extracting the maximum capacity from Co_3O_4, resulting in electrodes whose surfaces, both internal and external, are accessible to the electrolyte. The electrochemical performance of the composite material is promising with a volumetric capacity of 60.0 C/cm^3 and a specific capacity of 542.3 C/g, corresponding to 682.0 C/g of the constituent Co_3O_4. With a low equivalent series resistance of 0.9 Ω, the Co_3O_4/LSG electrode is able to maintain 113.1% of its original capacity after 10,000 cycles. This work provides new insights into the design of high-performance carbon/metal oxide nanocomposites for next-generation energy storage devices.

1 Introduction

Rapid improvements in consumer electronics and electric vehicles drive the need for reliable energy storage systems with enhanced energy and power densities. Because of their excellent electrochemical properties, supercapacitors have been recognized as one of the most promising energy storage systems.

Address correspondence to kaner@chem.ucla.edu

They exhibit intermediate properties between those of traditional capacitors and chemical batteries [1]. In addition, they are likely to play an important role in the future of energy storage thanks to their high power density, long cycle life, and ability to work at low temperatures [2]. These characteristics make supercapacitors the technology of choice for consumer electronics, backup power, and regenerative braking. In addition, battery/supercapacitor combinations are now under investigation as promising power sources for electric vehicles [1, 3, 4].

There are two main types of supercapacitors distinguished by their charge storage mechanism [5]. The first, called an electric double-layer capacitor (EDLC), stores energy electrostatically through adsorption of electrolyte ions on the electrode surfaces. The second type of supercapacitor is composed of pseudo-capacitive or battery-like materials. Energy is stored via fast and reversible redox reactions occurring primarily on their surfaces. Following recommendations from Brousse et al. [6], it is necessary to distinguish between normal pseudo-capacitive materials and battery-like materials. According to Brousse et al. [6], the term "pseudo-capacitive" can only be used when a redox active material has the electrochemical signature of a capacitive carbon electrode. A typical example under this category is ruthenium oxide, whose rectangular cyclic voltammogram (CV) profile over a large voltage window is the origin of the term "pseudo-capacitance". Other metal oxides/hydroxides showing clear redox peaks during charge and discharge can no longer be described as pseudo-capacitors, but instead have characteristics similar to those of batteries. To put things in perspective, capacity in coulombs per gram (C/g) should be used instead of capacitance in farads per gram (F/g) for the evaluation of the performance of such battery-like electrodes.

Carbon materials with large specific surface areas, such as activated carbons, carbon nanotubes, and graphene, are normally used in EDLCs [7]. Their high surface area provides a large number of sites for charge storage through ion adsorption. The surface area of the carbon materials can be further optimized by introducing well-aligned pore structures with methods that include templating and chemical etching [8]. Among all the carbon materials, graphene has shown the greatest promise because of its excellent electrical conductivity, good mechanical properties, and extraordinarily high surface area [9–11]. While graphene supercapacitors have demonstrated excellent electrochemical properties, practical applications of carbon materials are still limited by their relatively low energy density. On the other hand, pseudo-capacitive and battery-like materials can exhibit up to ten times higher capacity than carbonaceous materials thanks to energy-dense Faradaic reactions. Typical electrode materials for the second type of supercapacitors consist of metal oxides and nitrides [12–17] and conducting polymers [18], or combinations thereof. Because of its high theoretical capacity, Co_3O_4 is a very attractive material for energy storage. In addition, it is promising for mass production due to its abundance and low cost. However, like most other metal oxides, Co_3O_4 suffers from low electronic conductivity and limited stability, losing its capacity rapidly upon cycling.

In order to improve the electrochemical performance of metal oxides, morphology control, and pore size design are of paramount importance. A rationally controlled structure may facilitate ion diffusion and improve the mechanical properties of the material and, therefore, its energy efficiency. A number of research groups have synthesized Co_3O_4 with different nanostructures, such as nanowires [19], nanotubes [20], nanobelts [21], nanoneedles [22], nanorods [23], and hollow nanoparticles [24]. Synthesis of layered Co_3O_4 by chemical exfoliation is also reported to enhance its surface area and improve ion diffusion [8, 25]. Among these, the hollow nanoparticle architecture is most desirable for supercapacitor applications. The hollow structure not only provides an outside surface for charge storage, but also makes the inner surface accessible, resulting in more active sites for redox reactions. In addition, the hollow structure lowers the diffusion length of ions and improves the power density of the system. Moreover, less dead mass will be involved and the materials will be more effectively used. Representative methods for the fabrication of hollow Co_3O_4 include hard templates [26], soft templates [27], the nanoscale Kirkendall effect [24], and Ostwald ripening methods [28].

Although the structure of Co_3O_4 can be tailored with high precision, its low conductivity of 10^{-4} to

10^{-2} S/cm [13] hinders Co_3O_4 from achieving its theoretical capacity. Besides, the poor mechanical properties of metal oxides make them prone to degradation during repeated charging and discharging. To overcome these drawbacks, metal oxides are often combined with carbon nanomaterials to form new composite electrodes with chemical and physical properties that are distinct from their individual components [29–31]. In these composites, carbon provides a conductive network, allowing fast electron transport and high power output, while the metal oxide boosts the energy density of the entire system thanks to its high specific capacity. Previous work from our group shows that the laser scribing of graphite oxide (GO) films results in three-dimensional (3D) macroporous graphene electrodes, called laser-scribed graphene (LSG) [9]. LSG exhibits an excellent electrical conductivity of more than 1,700 S/m and a large surface area in excess of 1,500 m^2/g. These features make LSG an ideal candidate for the fabrication of metal oxide/carbon composite electrodes.

Inspired by these features, we developed a hybrid system comprising hollow Co_3O_4 nanoboxes and LSG macroporous electrodes. Here, the hollow Co_3O_4 nanoboxes are produced by using the nanoscale Kirkendall effect [24], which involves low temperature recrystallization of cobalt acetate followed by slow calcination. These hollow Co_3O_4 structures are embedded into the LSG framework by mixing the metal oxide with GO and converting the composite into Co_3O_4/LSG via a laser scribing technique, as shown in Fig. 1. A high specific surface area of 357 m^2/g was measured for the composite material. In such a porous structure, the LSG performs as a 3D conductive scaffold for the metal oxide, expediting electron transport by lowering the equivalent series resistance (ESR) to < 1 Ω. The LSG also functions as a 3D matrix over which the metal oxide is anchored, allowing for improved electrochemical properties of Co_3O_4 and preventing the nanoboxes from aggregating. The Co_3O_4 not only makes up for the relatively low capacity of LSG, but also offers more active sites for redox reactions, leading to electrodes with both enhanced energy and power density. With the synergistic effects between the metal oxide and LSG, an areal capacity of 60.0 mC/cm^2 is reached, which is 8 times higher than that of pure LSG. These features make hollow Co_3O_4/LSG a promising candidate for the next generation of high-performance energy storage electrodes. This work also provides new insights into our understanding of the properties of metal oxides and lays down new strategies for designing improved metal oxide-based energy storage devices.

2 Experimental

2.1 Preparation of hollow Co_3O_4 nanoboxes

In a typical experiment, 0.8 g of $Co(CH_3COO)_2{\cdot}4H_2O$ is dissolved in 500 mL [24] of cold ethanol and the solution is kept at −5 ˚C. After several weeks, the precipitate is collected and washed with ethanol by centrifugation, followed by drying overnight in a vacuum oven. The powder is then heated to 300 ˚C

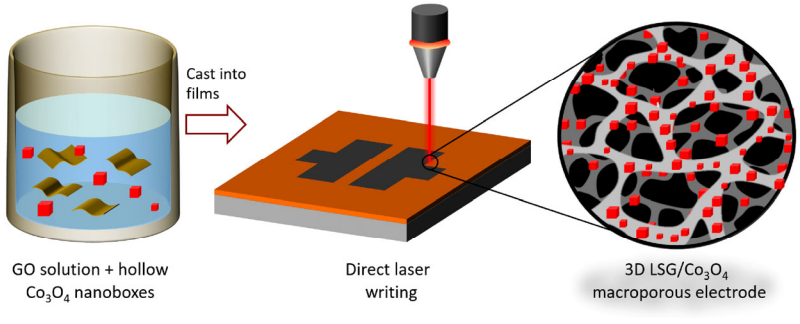

Figure 1 Fabrication of hollow Co_3O_4/LSG composite electrodes. First, Co_3O_4 nanoboxes are made with a combination of recrystallization and calcination steps. The as-prepared Co_3O_4 boxes are mixed with GO, coated onto a substrate, and then scribed with a CO_2 laser to produce the Co_3O_4/LSG composite, which is confirmed by a color change from light gray to black. The resulting electrode features a 3D graphene matrix with a high surface area where the Co_3O_4 nanoboxes are uniformly anchored to its surface, allowing for efficient charge storage.

at a rate of 1 ℃/min and calcinated for 10 min to complete the conversion to Co_3O_4.

2.2 Synthesis of the hollow Co_3O_4/LSG composite

The as-prepared Co_3O_4 nanoboxes are mixed with freeze-dried GO and water, stirred and sonicated. This forms a homogeneous solution, which is then drop-cast onto stainless steel substrates and dried overnight. A CO_2 laser (Full spectrum laser, MLE-40, 10.6 μm) is used to scribe the film, turning it from light gray Co_3O_4/GO to black Co_3O_4/LSG (Fig. S1 in the Electronic Supplementary Material (ESM)).

2.3 Fabrication of the commercial Co_3O_4/LSG composite

The same ratio of the commercial Co_3O_4 is mixed with freeze-dried GO and water, stirred and sonicated. The drop-casting and laser scribing procedure as described above is then used to make the commercial Co_3O_4/LSG composite.

2.4 Electrochemical measurements

A three-electrode system was used to evaluate the performance of the Co_3O_4, the LSG, and the Co_3O_4/LSG composite materials. In this system, platinum foil functions as the counter electrode, a Hg/HgO electrode as the reference electrode, and a 6.0 M KOH solution is used as the electrolyte. The electrochemical performance was evaluated by CV, galvanostatic charge/discharge cycles and electrochemical impedance spectroscopy (EIS) using a Biologic VMP3 electrochemical workstation. The Co_3O_4/LSG films were cut into 0.5 cm × 0.5 cm squares, made into electrodes by connecting with copper tape and then passivated with 5-minute epoxy (Devcon).

2.5 Characterization

The morphology of both metal oxide and composite films were studied using a field emission scanning electron microscope (FESEM, JEOL JSM-6700F FE-SEM) and a transmission electron microscope (TEM, T12 Quick CryoEM and CryoET (FEI)). The crystalline nature of the materials was further characterized by X-ray diffraction (XRD, Bruker DUO Apexll CCD-single crystal X-ray Diffractometer). Elemental analysis was carried out using X-ray photoelectron spectroscopy (XPS, Kratos Axis Ultra DLD spectrometer). The surface area of the composite material was analyzed using the methylene blue absorption method and the absorbance was measured by UV–vis spectroscopy (Shimadzu UV/Vis/NIR spectrophotometer, UV-3101PC).

3 Results and discussion

3.1 Fabrication of hollow Co_3O_4/LSG composites

The Co_3O_4 nanoboxes are fabricated in a two-step process, in which cobalt acetate is recrystallized in cold ethanol followed by calcination at a slow rate. The hollow structure is obtained as a result of the difference in the diffusion rates of C, H, and Co atoms from cobalt acetate during the slow heating process, a phenomenon known as the nanoscale Kirkendall effect [32]. The process can be described as follows: The C, H, and Co on the surface are oxidized to form a layer of Co_3O_4. At the same time, the C, H, and Co from the inside will constantly diffuse to the surface and react with oxygen, continuously forming cavities and eventually leading to the formation of the hollow Co_3O_4 structure. In order to fabricate the electrodes, a homogeneous solution of Co_3O_4 and graphite oxide is made by stirring and sonicating an equal amount (w/w) of metal oxide and freeze-dried GO in deionized (DI) water. The solution is coated onto stainless steel foil and allowed to dry overnight under ambient conditions. Next, laser irradiation of the coated Co_3O_4/GO films using a CO_2 laser table (10.6 μm) running at a power of 6 W is applied. The laser triggers the deoxygenation of GO in the composite through a photothermal process. This is manifested by a change in the color of the composite film from light gray to gray-black, indicating the successful transition from Co_3O_4/GO to a Co_3O_4/LSG nanocomposite.

3.2 Characterization of hollow Co_3O_4 nanoboxes and Co_3O_4/LSG composite electrodes

The crystal structure of the Co_3O_4 nanoboxes was investigated using XRD. As Fig. 2(a) shows, the XRD

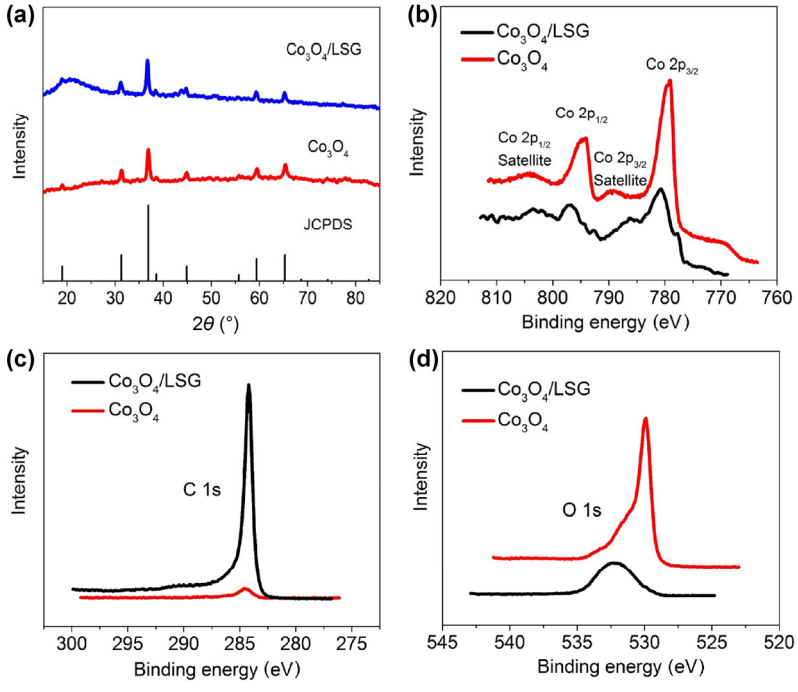

Figure 2 (a) XRD patterns of the as-prepared hollow Co_3O_4 and Co_3O_4/LSG, compared with the JCPDS pattern, confirming that the material is Co_3O_4 with a cubic spinel structure. (b) Co 2p XPS spectra confirm that Co is in both the metal oxide and composite. (c) XPS of the C 1s peak indicates the presence of C (as LSG) in the composite. (d) O 1s XPS spectra of Co_3O_4 and Co_3O_4/LSG.

pattern has major peaks positioned at 2θ = 19.0°, 31.3°, 36.9°, 38.6°, 44.8°, 59.4°, and 65.3°, which matches well with the Co_3O_4 cubic spinel structure (JCPDS card no. 42-1467) [20]. This confirms the successful oxidation of cobalt acetate to Co_3O_4 during calcination. XRD patterns of Co_3O_4/LSG nanocomposites show the same peaks, while maintaining the same position and intensity ratio except for a broad peak around 25°, which indicates the formation of graphene. The similarity in the XRD patterns for the metal oxide and the composite indicates that the metal oxide material remains as Co_3O_4 after laser processing.

XPS spectra of both the metal oxide and the composite provide additional confirmation of the production of the desired materials. As shown in Fig. 2(b), both samples exhibit XPS peaks at 779.7 eV for Co $2p_{3/2}$ and 794.7 eV for Co $2p_{1/2}$, which is consistent with literature values [33] and confirms the existence of Co_3O_4 in both samples. In the composite material, metal oxide nanoboxes are embedded into LSG, causing a much weaker signal for the Co 2p peaks. In addition, Fig. 2(c) shows photoemission peaks at 284.6 and 284.2 eV, corresponding to the carbon in LSG and ambient CO_2, respectively. When compared with the C 1s spectra of Co_3O_4/GO (Fig. S2 in the ESM), the LSG exhibits no apparent peaks for oxygen containing groups, confirming the conversion from GO to graphene. Furthermore, the O 1s peaks in the metal oxide sample appear at binding energies of 529.9 and 531.5 eV, in good agreement with the literature values for Co_3O_4 [33]. The broad emission peak of the composite at 532.3 eV is related to the oxygen functional groups remaining in the LSG network, overriding the signal from the metal oxide oxygen. Raman spectra were also collected for LSG and the composite materials, which both show typical peaks for graphene (Fig. S3 in the ESM). The D:G ratio is between 1.4 and 1.6, indicating that the samples are rich in edges [34].

To confirm the unique structure of the Co_3O_4, TEM was used. The TEM image in Fig. 3(a) reveals the distinct hollow nature of the as-prepared Co_3O_4, with particle sizes ranging from a hundred to a few hundred nanometers. The morphology of the metal oxide nanoboxes was further investigated by SEM. As shown in Figs. 3(b) and 3(c), the vacancy inside the nanoboxes

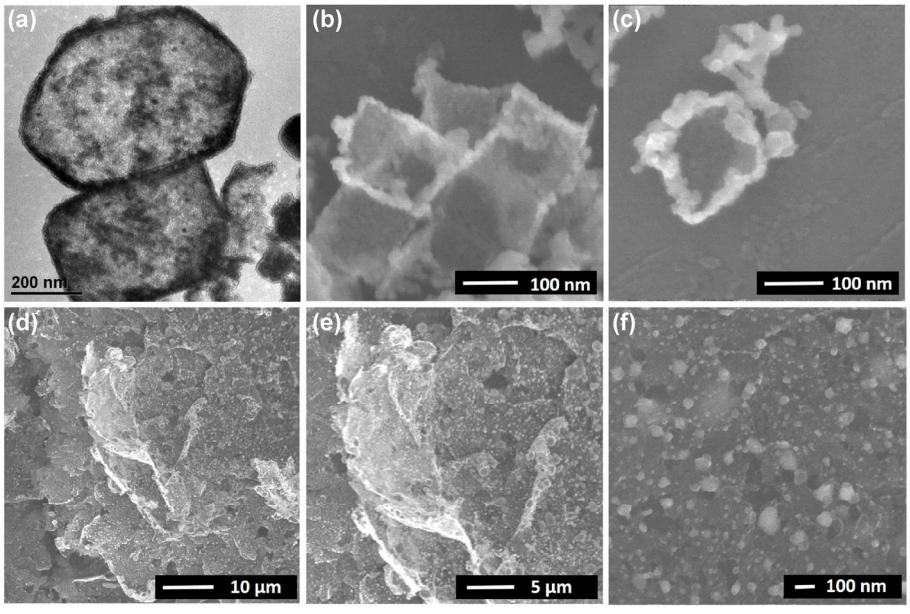

Figure 3 Electron microscope images of Co_3O_4 nanoboxes and the Co_3O_4/LSG composite. (a) A TEM image shows the hollow structure of the Co_3O_4 nanoboxes. (b) and (c) SEM images showing the hollow morphology of the nanoboxes. (d)–(f) SEM images of the Co_3O_4/LSG composite, indicating that the metal oxide is homogeneously dispersed in the LSG framework.

is clearly displayed through an open end. Benefiting from the hollow structure of the Co_3O_4, the materials will have more surface area for redox reactions, fast ion diffusion, and a decreased amount of useless dead mass. Figures 3(d) and 3(e) indicate that embedding Co_3O_4 into an LSG electrode results in the uniform distribution of the nanoboxes on the graphene matrix with the box shape maintained after the process of laser scribing. Graphene serves as a large flexible carpet onto which the metal oxide nanoboxes can be anchored to form a stable matrix with no sign of metal oxide aggregation, preserving the surface area of the hollow Co_3O_4. The surface area is further enhanced by the intrinsic ultrahigh surface area of the LSG structure. Additionally, this carbon scaffold serves as a conductive holder for the metal oxide, providing superhighways for electrons and enabling fast charge transfer. Furthermore, the porous nature of the composite electrode provides tunnels for fast ion diffusion, which will improve the power output of the system.

3.3 Electrochemical properties of the hollow Co_3O_4 nanoboxes and the Co_3O_4/LSG composite

To test the electrochemical performance of the as-prepared Co_3O_4 nanoboxes and the Co_3O_4/LSG composite, a three-electrode measurement was carried out, in which a Hg/HgO electrode was used as the reference and 6.0 M KOH as the electrolyte. During the test, typical Faradaic peaks were observed in the CV curves from samples containing Co_3O_4 (Fig. 4(a)). These peaks arise from the redox reactions shown in Eqs. (1) and (2) [13].

$$Co_3O_4 + OH^- + H_2O \leftrightarrow 3CoOOH + e^- \quad (1)$$

$$3CoOOH + 3OH^- \leftrightarrow 3CoO_2 + 3H_2O + 3e^- \quad (2)$$

Much higher currents for both the Co_3O_4 nanobox and the Co_3O_4/LSG composite are observed relative to the pure LSG, owing to the very large specific capacity of cobalt oxide. With LSG as a 3D holder, the Co_3O_4 is less likely to aggregate and maintain its hollow structure. Thanks to the unique structure, the electrolyte ions do not have to diffuse all the way into the bulk material and surface reactions take place instead, resulting in less apparent redox peaks. Moreover, both LSG and hollow Co_3O_4 contribute to a relatively high surface area (357 m^2/g), which gives rise to a large double layer capacitance. As a result, the CV curve of the composite material is more rectangular,

while the redox peaks are hidden due to overlapping with the double-layer current. Interestingly, the composite CV also exhibits a much larger CV area than the metal oxide. The improved electrochemical performance is obvious from capacity calculations as shown in Fig. 4(b). The capacity of the composite material is 60.0 mC/cm^2, which is 6 times larger than the pure metal oxide and 8 times larger than graphene. When converted to volumetric capacity, the composite demonstrates a capacity of 68.5 C/cm^3, compared to 6.0 C/cm^3 for the LSG electrodes. This is also superior to previously reported graphene/Co_3O_4 composite electrodes, such as 15.4 C/cm^3 (calculated based on a capacitance of 30.8 F/cm^3 and a 0.5 V voltage window) reported by Mazloumi et al. [35]. Based on the active mass of the electrode, a specific capacity of 542.3 C/g is derived for our composite material, which is superior to the value of 109.0 C/g reported for Co_3O_4/carbon nanoneedles [36], 293 C/g for Co_3O_4/carbon nanofibers [37], 324.5 C/g for Co_3O_4/MWCNTs [38], and 367.3 C/g for Co_3O_4/graphene [39] (the values have all been recalculated based on the reported capacitance and potential window). When subtracting the capacitance of graphene, the specific capacity attributed to just the constituent Co_3O_4 is calculated to be 682.0 C/g based on 77% mass loading (calculated by thermogravimetric analysis (TGA) of the Co_3O_4/LSG sample, see Fig. S4(a) in the ESM). This value demonstrates the good charge storage capability of hollow Co_3O_4 nanoboxes and shows a clear improvement over other hollow structures, such as 329.5 C/g for Co_3O_4 nanotubes [40]. This excellent electrochemical performance can be attributed to the increased surface area of the nanoboxes, enabling maximum utilization of the Faradaic properties of Co_3O_4 and resulting in electrodes with ultrahigh specific capacity. In addition, the synergetic interactions between LSG and Co_3O_4 help improve the overall performance of the composite. In such a hybrid material system, the LSG keeps the Co_3O_4 nanoboxes from aggregating, maintaining the intrinsic properties, while also contributing a significant amount of EDLC capacitance. The electrically conductive framework of LSG enhances the charge transfer from the metal oxide, more fully utilizing the

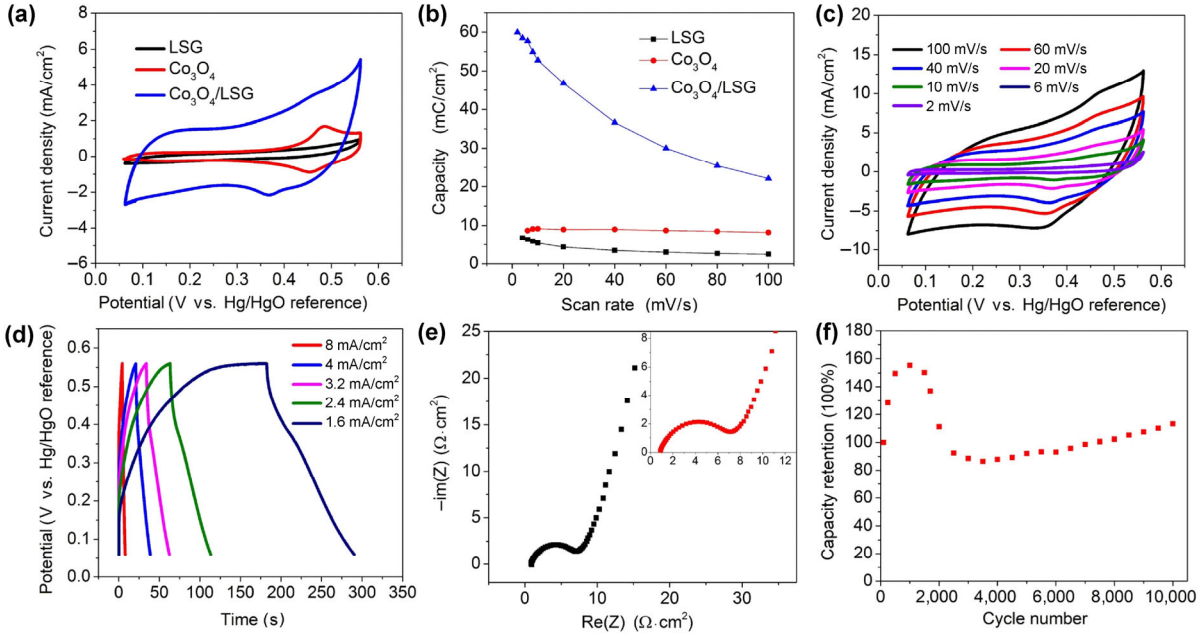

Figure 4 (a) CV comparison of the Co_3O_4/LSG composite, LSG, and pure metal oxide at a scan rate of 20 mV/s. (b) Areal capacity comparing the Co_3O_4/LSG composite, LSG, and pure metal oxide at different scan rates. (c) CVs of the Co_3O_4/LSG composite at scan rates ranging from 2 to 100 mV/s, displaying similar shapes. (d) Galvanostatic charge/discharge curves of the Co_3O_4/LSG composite at different current densities (8 to 1.6 mA/cm^2). (e) Nyquist plot of the Co_3O_4/LSG composite demonstrating low resistance for the electrode material, the electrolyte, and the inter-particle contacts, as well as low internal charge transfer and ion diffusion resistance. (f) Capacity retention as a function of cycle number, indicating that the Co_3O_4/LSG composite is able to maintain its capacity for at least 10,000 cycles.

potential capacity of Co_3O_4. The porous structure of the film also facilitates ion migration in the electrolyte. As a result, the conductivity of the whole system, both electronic and ionic, is improved. This is also reflected in the CV and constant current change and discharge curves (CC) curves shown in Figs. 4(c) and 4(d). Even at a high scan rate of 100 mV/s, the shape of the LSG/Co_3O_4 composite CV is similar to those at lower scan rates. Similarly, the charging/discharging time is almost inversely proportional to the current density and there is no apparent *iR* drop in Fig. 4(d), indicating fast charge propagation and good power output. The internal resistance shown in the Nyquist impedance plot in Fig. 4(e) provides further evidence for the high power density of this composite electrode. As explained in Ref. [41], the ESR measured as the curve's intercept with the *x*-axis, including the electrode material, the electrolyte, and the inter-particle contacts, is as low as 0.9 Ω in the figure. In addition, there is no 45° diagonal in the plot, suggesting a good ion diffusion process. The semi-circle observed corresponds to a Faradaic resistance [41] of less than 8 Ω, related to the redox reaction and charge transfer. At the same time, the electrochemical processes within the Co_3O_4/LSG composite are highly reversible as the electrode maintains 113.1% of its original capacity after 10,000 cycles (Fig. 4(f)) without the breakdown of the hollow structure (Fig. S5 in the ESM). From the first cycle, the capacity keeps increasing reaching a maximum at ~ 1,000 cycles. This can be attributed to electrochemical activation processes commonly encountered in carbon and metal oxide electrodes.

In order to understand the role of the hollow structure of the Co_3O_4 nanoboxes, we fabricated composite electrodes using LSG in combination with commercially available round and solid Co_3O_4 particles at the same mass loading. The electrochemical performance of these composite electrodes is presented in Fig. 5. The current density of the hollow metal oxide nanoboxes is much larger than commercial Co_3O_4, both in its pure form (Fig. 5(a)) and in a composite electrode (Fig. 5(b)). The CV curve of the composite material is more rectangular than the composite containing commercial Co_3O_4 due to fast surface

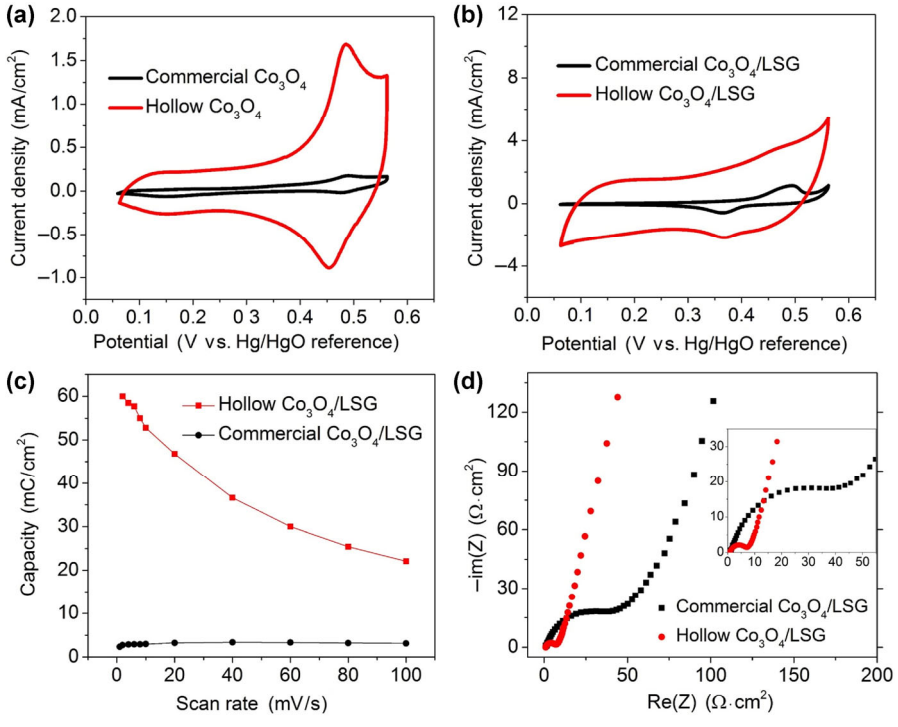

Figure 5 (a) A CV comparison of commercial Co_3O_4 and as-prepared Co_3O_4 hollow nanoboxes at 20 mV/s. (b) A CV comparison of commercial and hollow Co_3O_4/LSG composites at 20 mV/s. (c) Areal capacity comparing commercial and hollow Co_3O_4/LSG composites at scan rates ranging from 2 to 100 mV/s. (d) Nyquist plots of the commercial and hollow Co_3O_4/LSG composites, showing lower charge transfer and ion diffusion resistance of the hollow Co_3O_4/LSG composite.

reactions and large double layer capacitance from the hollow structure. The corresponding capacities derived from the CV curves are shown in Fig. 5(c), which agrees very well with the results discussed above. The excellent performance of our materials can be attributed to the hollow structure of Co_3O_4, as explained in the schematic illustration shown in Fig. 6. The hollow metal oxide supplies not only accessible outer surfaces, but also makes the inside surfaces available, offering more surface area for ion absorption and active sites for redox reactions. Here, all the materials are expected to be used more efficiently, leaving behind less dead mass. In contrast to the solid morphology, ions are able to move readily through the open cavities in the hollow nanoboxes, leading to enhanced wetting properties. In addition, the ion diffusion length and charge transfer distance are shortened since only near surfaces are involved, further expediting ion migration. These explanations are backed up by the EIS measurements (Fig. 5(e)). In contrast to the hollow Co_3O_4/LSG composite, the commercial Co_3O_4/LSG composite exhibits a much larger semi-circle, which means a significant charge transfer resistance. The commercial composite also shows an obvious 45° diagonal between 50 and 70 Ω, due to the more difficult ion diffusion processes. These results demonstrate the outstanding electrochemical performance of hollow Co_3O_4 nanoboxes embedded in a 3D macro-porous graphene matrix (Fig. S6 in the ESM).

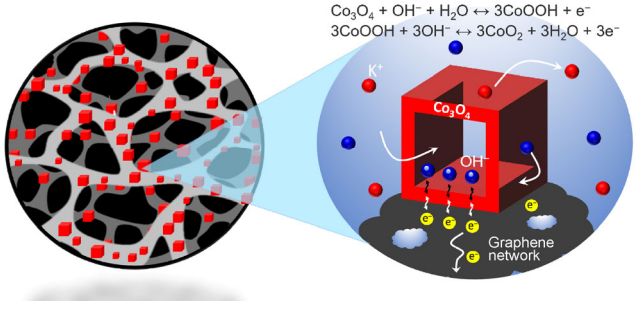

Figure 6 Schematic illustration showing the advantage of using hollow Co_3O_4 nanoboxes. I. Both the inside and the outside surfaces of the metal oxide can be utilized, providing more sites for redox reactions and ion absorption. II. Ions can diffuse freely throughout the cavity to the surfaces, easing the wetting of the material and enhancing the power output. III. More active materials are accessible compared to a solid morphology, thus lowering the amount of dead mass.

4 Conclusions

In this study, we have demonstrated a facile method to fabricate hollow Co_3O_4/LSG electrodes. Hollow Co_3O_4 nanoboxes are made via low-temperature recrystallization, followed by a calcination process. The as-prepared metal oxide is then mixed with a GO solution, cast as a film, and the GO component is photothermally reduced to LSG using a CO_2 laser. Thanks to the unique structure of the hollow Co_3O_4 nanoboxes and a synergetic effect between the metal oxide and the LSG matrix, the composite exhibits a large surface area, good ion diffusion, and fast charge transfer, leading to excellent electrochemical performance. This composite electrode demonstrates ultrahigh specific capacity, low internal resistance, and excellent cycling stability. These interesting features of hollow Co_3O_4/LSG offer a great opportunity to increase the energy density of state-of-the-art supercapacitors.

Acknowledgements

The authors would like to acknowledge financial support from Nanotech Energy, Inc. (R. B. K.) and the China Scholarship Council (M. L.). Special thanks to Michael Yeung for help with calcination of the electrode materials.

Electronic Supplementary Material: Supplementary material (related calculations, SEM images, TGA measurements, Raman and XPS spectra) is available in the online version of this article at https://doi.org/10.1007/s12274-017-1914-7.

References

[1] Simon, P.; Gogotsi, Y. Materials for electrochemical capacitors. *Nat. Mater.* **2008**, *7*, 845–854.

[2] Burke, A. R&D considerations for the performance and application of electrochemical capacitors. *Electrochim. Acta* **2007**, *53*, 1083–1091.

[3] Miller, J. R.; Burke, A. F. Electrochemical capacitors: Challenges and opportunities for real-world applications. *J. Electrochem. Soc. Interface* **2008**, *17*, 53–57.

[4] Simon, P.; Gogotsi, Y.; Dunn B. Where do batteries end and supercapacitors begin? *Science* **2014**, *343*, 1210–1211.

[5] Winter, M.; Brodd R. J. What are batteries, fuel cells, and supercapacitors? *Chem. Rev.* **2004**, *104*, 4245–4270.

[6] Brousse, T.; Bélanger, D.; Long, J. W. To be or not to be pseudocapacitive? *J. Electrochem. Soc.* **2015**, *162*, 5185–A5189.

[7] Zhang, L. L.; Zhao X. S. Carbon-based materials as supercapacitor electrodes. *Chem. Soc. Rev.* **2009**, *38*, 2520–2531.

[8] Kou, T. Y.; Yao, B.; Liu, T. Y.; Li, Y. Recent advances in chemical methods for activating carbon and metal oxide based electrodes for supercapacitors. *J. Mater. Chem. A* **2017**, *5*, 17151–17173.

[9] El-Kady, M. F.; Strong, V.; Dubin, S.; Kaner, R. B. Laser scribing of high-performance and flexible graphene-based electrochemical capacitors. *Science* **2012**, *335*, 1326–1330.

[10] Shao, Y. L.; El-Kady, M. F.; Lin, C. W.; Zhu, G. Z.; Marsh, K. L.; Hwang, J. Y.; Zhang, Q. H.; Li, Y. G.; Wang, H. Z.; Kaner, R. B. 3D freeze-casting of cellular graphene films for ultrahigh-power-density supercapacitors. *Adv. Mater.* **2016**, *28*, 6719–6726.

[11] Wang, L. J.; El-Kady, M. F.; Dubin, S.; Hwang, J. Y.; Shao, Y. L.; Marsh, K.; McVerry, B.; Kowal, M. D.; Mousavi, M. F.; Kaner, R. B. Flash converted graphene for ultra-high power supercapacitors. *Adv. Energy Mater.* **2015**, *5*, 1500786.

[12] El-Kady, M. F.; Ihns, M.; Li, M. P.; Hwang, J. Y.; Mousavi, M. F.; Chaney, L.; Lech, A. T.; Kaner, R. B. Engineering three-dimensional hybrid supercapacitors and microsupercapacitors for high-performance integrated energy storage. *Proc. Natl. Acad. Sci. USA* **2015**, *112*, 4233–4238.

[13] Zhi, M. J.; Xiang, C. C.; Li, J. T.; Li, M.; Wu, N. Q. Nanostructured carbon–metal oxide composite electrodes for supercapacitors: A review. *Nanoscale* **2013**, *5*, 72–88.

[14] Wang, L.; Ji, H. M.; Wang, S. S.; Kong, L. J.; Jiang, X. F.; Yang, G. Preparation of Fe_3O_4 with high specific surface area and improved capacitance as a supercapacitor. *Nanoscale* **2013**, *5*, 3793–3799.

[15] Chen, Y. L.; Wang Y.; Sun, P.; Yang, P. H.; Du, L. H.; Mai, W. J. Nickel oxide nanoflake-based bifunctional glass electrodes with superior cyclic stability for energy storage and electrochromic applications. *J. Mater. Chem. A* **2015**, *3*, 20614–20618.

[16] Lian, C.; Wang, Z.; Lin, R.; Wang, D. S.; Chen, C.; Li, Y. D. An efficientfficient, controllable and facile two-step synthesis strategy: Fe_3O_4@RGO composites with various Fe_3O_4 nanoparticles and their supercapacitance properties. *Nano Res.* **2017**, *10*, 3303–3313.

[17] Zhang, X. J.; Shi, W. H.; Zhu, J. X.; Zhao, W. Y.; Ma, J.; Mhaisalkar, S.; Maria, T. L.; Yang, Y. H.; Zhang, H.; Hng, H. H. et al. Synthesis of porous NiO nanocrystals with controllable surface area and their application as supercapacitor electrodes. *Nano Res.* **2010**, *3*, 643–652.

[18] Wang, Y. R.; Wei, H. G.; Wang, J. M.; Liu, J. R.; Guo, J.; Zhang, X.; Weeks, B. L.; Shen, T. D.; Wei, S. Y.; Guo, Z. H. Electropolymerized polyaniline/manganese iron oxide hybrids with an enhanced color switching response and electrochemical energy storage. *J. Mater. Chem. A* **2015**, *3*, 20778–20790.

[19] Li, Y. G.; Tan, B.; Wu, Y. Y. Mesoporous Co_3O_4 nanowire arrays for lithium ion batteries with high capacity and rate capability. *Nano Lett.* 2008, *8*, 265–270.

20] Du, N.; Zhang, H.; Chen, B. D.; Wu, J. B.; Ma, X. Y.; Liu, Z. H.; Zhang, Y. Q.; Yang, D. R.; Huang, X. H.; Tu, J. P. Porous Co_3O_4 nanotubes derived from $Co_4(CO)_{12}$ clusters on carbon nanotube templates: A highly efficient material for Li-battery applications. *Adv. Mater.* 2007, *19*, 4505–4509.

[21] Tian, L.; Zou, H. L.; Fu, J. X.; Yang, X. F.; Wang, Y.; Guo, H. L.; Fu, X. H.; Liang, C. L.; Wu, M. M.; Shen, P. K. et al. Topotactic conversion route to mesoporous quasi-single-crystalline Co_3O_4 nanobelts with optimizable electrochemical performance. *Adv. Funct. Mater.* 2010, *20*, 617–623.

[22] Lou, X. W.; Deng, D.; Lee, J. Y.; Feng, J.; Archer, L. A. Self-supported formation of needlelike Co_3O_4 nanotubes and their application as lithium-ion battery electrodes. *Adv. Mater.* 2008, *20*, 258–262.

[23] Cheng, G. H.; Kou, T. Y.; Zhang, J.; Si, C. H.; Gao, H.; Zhang, Z. H. O_2^{2-}/O^- functionalized oxygen-deficient Co_3O_4 nanorods as high performance supercapacitor electrodes and electrocatalysts towards water splitting. *Nano Energy* **2017**, *38*, 155–166.

[24] Du, W.; Liu, R. M.; Jiang, Y. W.; Lu, Q. Y.; Fan, Y. Z.; Gao, F. Facile synthesis of hollow Co_3O_4 boxes for high capacity supercapacitor. *J. Power Sources* **2013**, *227*, 101–105.

[25] Xuan, L. Y.; Chen, L. Y.; Yang, Q. Q.; Chen, W. F.; Hou, X. H.; Jiang, Y. Q.; Zhang, Q.; Yuan, Y. Engineering 2D multi-layer graphene-like Co_3O_4 thin sheets with vertically aligned nanosheets as basic building units for advanced pseudocapacitor materials. *J. Mater. Chem. A* **2015**, *3*, 17525–17533.

[26] Xia, X. H.; Tu, J. P.; Wang, X. L.; Gu, C. D.; Zhao, X. B. Mesoporous Co_3O_4 monolayer hollow-sphere array as electrochemical pseudocapacitor material. *Chem. Commun.* **2011**, *47*, 5786–5788.

[27] He, T.; Chen, D.; Jiao, X.; Wang, Y. Co_3O_4 nanoboxes: Surfactant-templated fabrication and microstructure characterization. *Adv. Mater.* **2006**, *18*, 1078–1082.

[28] Wang, X.; Fu, H. B.; Peng, A. D.; Zhai, T. Y.; Ma, Y.; Yuan, F. L.; Yao, J. N. One-pot solution synthesis of cubic cobalt nanoskeletons. *Adv. Mater.* **2009**, *21*, 1636–1640.

[29] Hwang, J. Y.; El-Kady, M. F.; Wang, Y.; Wang, L. S.; Shao, Y. L.; Marsh, K.; Ko, J. M.; Kaner, R. B. Direct preparation and processing of graphene/RuO_2 nanocomposite electrodes for high-performance capacitive energy storage. *Nano Energy* **2015**, *18*, 57–70.

[30] Foo, C. Y.; Sumboja, A.; Tan, D. J. H.; Wang, J. X.; Lee, P. S. Flexible and highly scalable V_2O_5-rGO electrodes in an organic electrolyte for supercapacitor devices. *Adv. Energy Mater.* **2014**, *4*, 1400236.

[31] Peng, Y. T.; Chen, Z.; Wen, J.; Xiao, Q. F.; Weng, D.; He, S. Y.; Geng, H. B.; Lu, Y. F. Hierarchical manganese oxide/carbon nanocomposites for supercapacitor electrodes. *Nano Res*. **2011**, *4*, 216–225.

[32] Yin, Y.; Rioux, R. M.; Erdonmez, C. K.; Hughes, S.; Somorjai, G. A.; Alivisatos, A. P. Formation of hollow nanocrystals through the nanoscale Kirkendall effect. *Science* **2004**, *304*, 711–714.

[33] Xu, J. M.; Wu, J. S.; Luo, L. L.; Chen, X. Q.; Qin, H. B.; Dravid, V.; Mi, S. B.; Jia, C. L. Co_3O_4 nanocubes homogeneously assembled on few-layer graphene for high energy density lithium-ion batteries. *J. Power Sources* **2015**, *274*, 816–822.

[34] Ni, Z. H.; Wang, Y. Y.; Yu T.; Shen, Z. X. Raman spectroscopy and imaging of graphene. *Nano Res.* **2008**, *1*, 273–291.

[35] Mazloumi, M.; Shadmehr, S.; Rangom, Y.; Nazar, L. F.; Tang, X. W. Fabrication of three-dimensional carbon nanotube and metal oxide hybrid mesoporous architectures. *ACS Nano* **2013**, *7*, 4281–4288.

[36] Silva, R.; Pereira, G. M.; Voiry, D.; Chhowalla, M.; Asefa, T. Co_3O_4 nanoparticles/cellulose nanowhiskers-derived amorphous carbon nanoneedles: Sustainable materials for supercapacitors and oxygen reduction electrocatalysis. *RSC Adv.* **2015**, *5*, 49385–49391.

[37] Abouali, S.; Akbari Garakani, M.; Zhang, B.; Xu, Z. L.; Kamali Heidari, E.; Huang, J. Q.; Huang, J. Q.; Kim, J. K. Electrospun carbon nanofibers with *in situ* encapsulated Co_3O_4 nanoparticles as electrodes for high-performance supercapacitors. *ACS Appl. Mater. Interfaces* **2015**, *7*, 13503–13511.

[38] Wang, X. W.; Li, M. X.; Chang, Z.; Yang, Y. Q.; Wu, Y. P.; Liu, X. Co_3O_4@MWCNT nanocable as cathode with superior electrochemical performance for supercapacitors. *ACS Appl. Mater. Interfaces* **2015**, *7*, 2280–2285.

[39] Dong, X. C.; Xu, H.; Wang, X. W.; Huang, Y. X.; Chan-Park, M. B.; Zhang, H.; Wang, L. H.; Huang, W.; Chen, P. 3D graphene–cobalt oxide electrode for high-performance supercapacitor and enzymeless glucose detection. *ACS Nano* **2012**, *6*, 3206–3213.

[40] Xia, X. H.; Tu, J. P.; Mai, Y. J.; Wang, X. L.; Gu, C. D.; Zhao, X. B. Self-supported hydrothermal synthesized hollow Co_3O_4 nanowire arrays with high supercapacitor capacitance. *J. Mater. Chem.* **2011**, *21*, 9319–9325.

[41] Conway, B. E. *Electrochemical Supercapacitors: Scientific Fundamentals and Technological Applications*; Springer: New York, 2013.